THE JOURNAL OF PHYSICAL CHEMISTRY C

Article

pubs.acs.org/JPCC

Analysis of Photoacoustic Response from Gold−Silver Alloy Nanoparticles Irradiated by Short Pulsed Laser in Water

Ali Hatef,*[,†] Behafarid Darvish,[†] Adrien Dagallier,[‡] Yevgeniy R. Davletshin,[§] William Johnston,[†] J. Carl Kumaradas,[§] David Rioux,[‡] and Michel Meunier[‡]

[†]Nipissing Computational Physics Laboratory, Department of Computer Science and Mathematics, Nipissing University, 100 College Drive, North Bay, Ontario P1B 8L7, Canada

[‡]Laser Processing and Plasmonics Laboratory, Engineering Physics Department, École Polytechnique de Montréal, Montréal, Québec H3C 3A7, Canada

[§]Department of Physics, Ryerson University, 350 Victoria Street, Toronto, Ontario M5B 2K3, Canada

ABSTRACT: We perform a finite element-based numerical analysis to calculate the photoacoustic (PA) signal generated by spherical gold−silver (Au−Ag) alloy nanoparticles (NPs). These spherical particles are size-controlled and monodispersed, with tunable plasmonic resonance wavelength via change of the alloy composition. This enables their use in PA imaging as a contrast agent. This theoretical framework self-consistently solves the electromagnetic, thermodynamic and transient acoustic pressure physics using a multiphysics coupling approach. We model our system as an optically heterogeneous medium irradiated by a nanosecond laser pulse in the tissue therapeutic optical window (NIR irradiation, with wavelength of 800 nm). We calculate the PA signal generated by the photothermal expansion of both the particle and its surrounding medium. The results show the impact of the gold molar fraction (GMF) of Au−Ag alloy NPs on the PA signal for different NP sizes. We show that significantly stronger PA signals are achieved using Au−Ag alloy NPs (GMF = 0.55) in comparison with pure AuNPs (GMF = 1) and pure AgNPs (GMF = 0) of the same size and shape.

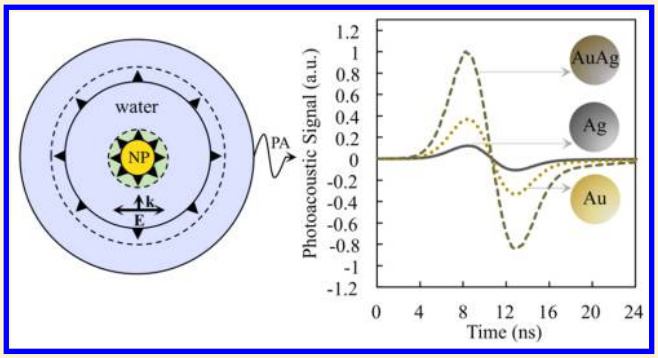

INTRODUCTION

Gold (Au) and silver (Ag) plasmonic nanoparticles (NPs) are widely used as contrast agents in thermal-expansion-based photoacoustic (PA) imaging technique[1] for biomedical applications. This technique utilizes the large optical absorption cross-section of these NPs due to their localized surface-plasmon resonance (LSPR).[2] In conventional approaches the NP geometry is designed and optimized to obtain strongest PA contrast and signal between regions with and without NPs. This is achieved by an efficient light-to-acoustic conversion, with optimization of NP's morphology, to have the highest rate of absorption to scattering.[3] So far, Au and Ag NPs of different shapes such as nanorods,[4] nanocages,[5] nanoshells,[6] and nanoplates[7] have been used as PA imaging contrast agents with high and tunable optical absorption cross sections in the near-infrared (NIR) region, where optical attenuation of biological tissues is relatively low.[8] These structures would be interesting to study because the shape strongly affects the position and strength of the plasmon resonance, which has a profound effect on the absorption cross-section; however, for practical applications, it is simpler and more convenient to produce spherical NPs.

Recently, Rioux et al.[9,10] developed a new synthesis protocol to produce monodispersed spherical Au−Ag alloy NPs with sizes from 30 to 150 nm in diameter. This protocol provides precise control on the shape, composition, and size of the alloy NPs during the synthesis. These alloy NPs should prove to be of a great interest in imaging due to their varying plasmon peak, and it would be interesting to study the behavior of these spherical alloy NPs of different sizes and compositions for PA imaging. Patskovsky et al.[11] have demonstrated how these Au−Ag alloy NPs satisfy the needs as large, size-controlled, and monodispersed spherical NPs for scattering-based biosensing and imaging markers in a biological medium. This paper is to show the absorption capability of these alloy NPs as a nanocontrast agent for PA imaging. To do this, we show the impact of gold molar fraction (GMF) and size of the Au−Ag alloy NP on the pressure wave generated by the thermal expansion of the alloy NP and its surrounding medium.

Our structure consists of Au−Ag alloy NP immersed in water because this medium has proven to be adequate for the modeling of laser processes occurring in a cellular medium.[8] Davletshin et al.[12] developed a finite element (FE) model for investigation of PA signal generation by the AuNP and its

Received: August 27, 2015
Revised: September 28, 2015

DOI: 10.1021/acs.jpcc.5b08359
J. Phys. Chem. C XXXX, XXX, XXX−XXX

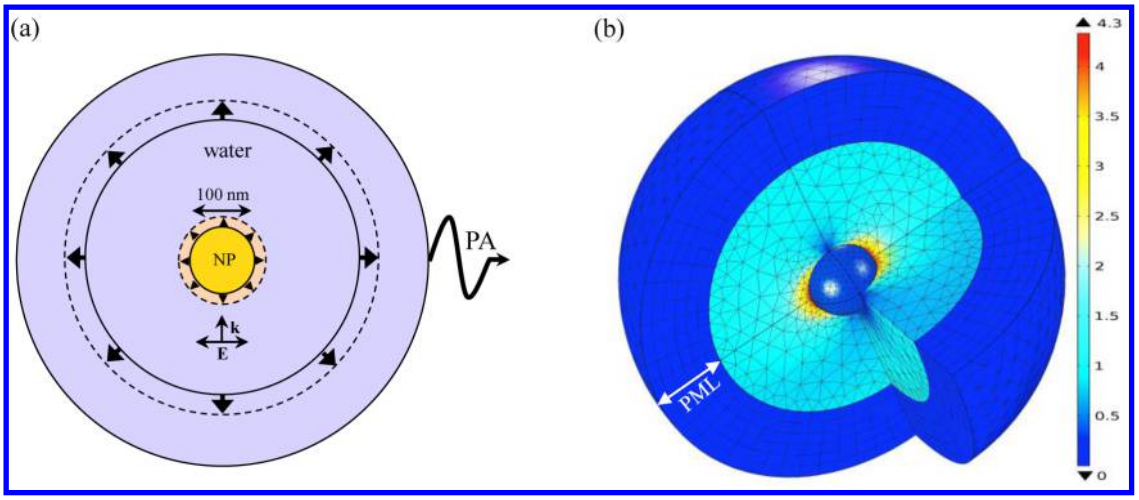

Figure 1. (a) 2D cross-section representation of the 3D geometry and boundary conditions of the computational model. The small arrows show the thermal expansion due to both alloy NP and the surrounding medium. The PA pressure is calculated on the outer boundary. (b) Plots of the relative electric field, $|E|/|E_0|$, where $|E|$ is the amplitude of the total electric field and E_0 is the amplitude of the incident electric field. The color legend shows the values of $|E|/|E_0|$.

environment. This computational model was adopted for evaluation of PA response of Au−Ag alloy NP and the surrounding medium (water in our case). The model is built for the analysis of PA signal by simulating light propagation in the medium and the associated thermo-acoustic signal generation. To do this, the following physical phenomena are one-way coupled: (1) optical properties of the Au−Ag alloy NP obtained from simulation of electromagnetic wave interaction with NP and coupled through resistive heating due to laser pulse to (2) transient heat transfer analysis and temperature increase calculation, where temperature is used as a coupling parameter, to (3) structural mechanics analysis for linear thermal expansion, stress, and strain calculation for the input as a boundary condition in acoustic-structure interaction for (4) acoustic pressure wave propagation modeling.

We have demonstrated that for the NPs of any size in the diameter range of 30 to 150 nm, the maximum absorption cross-section at wavelength of 800 nm occurs at GMF = 0.55, while the value increases by increasing the NP diameter. To avoid any phase change at the particle surface/water interface, the temperature at this interface needs to remain below the critical temperature of water ($0.9 \times T_{critical} = 580$ K).[13] Therefore, the maximum fluence that can be safely applied to each specific size of NPs with GMF of 0.55 has been calculated. Finally, the acoustic pressure signal is calculated for different sizes of NPs with GMFs of 0 (pure Ag), 0.55 (Au−Ag alloy), and 1 (pure Au). We show that irradiation of the Au−Ag alloy NPs by nanosecond pulse leads to achieving a significantly stronger PA signal in comparison with pure AuNPs and AgNPs of the same size and shape.

THEORY

Electromagnetic Wave Propagation. The source laser light is modeled as a linearly polarized plane wave at 800 nm. Assuming a time-harmonic electric field and $(1/\tau_w) \gg \omega$, where ω is the harmonic frequency of the electric field and $\tau_w = 5$ ns is the laser pulse width, the electric field distribution $\vec{E}$ is computed using the Helmholtz equation[14]

$$\nabla \times (\mu_r^{-1} \nabla \times \vec{E}) - k_0^2 \left(\varepsilon_r - j\frac{\sigma}{\omega \varepsilon_0}\right)\vec{E} = 0 \quad (1)$$

where ε_r, ε_0, μ_r, σ, and k_0 are the relative and vacuum permittivity, relative permeability, conductivity, and the wave-number, respectively. For Au−Ag alloy NPs, ε_r is a frequency-dependent complex permittivity and interpolated from an analytical model developed by Rioux et al.[10] The environment medium is water, which makes the obtained results more practical for biological applications.

Assuming a nondissipative host medium, the absorbed energy by the Au−Ag alloy NP is calculated as a resistive heating, Q_r

$$Q_r = \vec{J} \cdot \vec{E} \quad (2)$$

where $\vec{J}$ and $\vec{E}$ represent the current density and electric field strength, respectively.

Heat Transfer. For a nanosecond pulsed irradiation, the temperature rise, T, in NP and water is calculated by the heat diffusion equation[15]

$$\rho c \frac{\partial T}{\partial t} = \nabla \kappa \nabla T + Q_r * f(\tau_w) \quad (3)$$

where ρ, c, and κ are the density, heat capacity, and thermal conductivity, respectively. The function, $f(\tau_w)$, represents the temporal shape of the incident laser pulse, with the width, τ_w, defined as the full width at half-maximum (fwhm) of the Gaussian profile.

$$f(\tau_w) = \frac{1}{b\sqrt{2\pi}} e^{-(t-t_0)^2/2b^2} \quad (4)$$

where t_0 is the time position of the center of the peak and b is the standard deviation ($b = (\tau_w/2(2 \ln 2)^{1/2})$).

Structural Mechanics. The transient temperature rise of the Au−Ag alloy NP and its environment is used in structural mechanics model of linear thermal expansion to evaluate stress and strain tensor through the Duhamel−Hookes law[16]

$$\boldsymbol{s} = \boldsymbol{C}: (\boldsymbol{\epsilon} - \alpha(T - T_0)) \quad (5)$$

DOI: 10.1021/acs.jpcc.5b08359
J. Phys. Chem. C XXXX, XXX, XXX−XXX

Table 1. Parameters Have Been Used for PA FE Model

parameter	symbol	value
property X of alloy	X_{alloy}	$X_{Ag} \times GMF + X_{Au} \times (1 - GMF)$
density Ag	ρ_{Ag}	10490 kg/m^3
density Au	ρ_{Au}	19300 kg/m^3
density H_2O	ρ_{H_2O}	1000 kg/m^3
thermal conductivity Ag	κ_{Ag}	430 W/m/K
thermal conductivity Au	κ_{Au}	310 W/m/K
thermal conductivity H_2O	κ_{H_2O}	0.58 W/m/K
Poisson coefficient Ag	ν_{Ag}	0.37
Poisson coefficient Au	ν_{Au}	0.42
Young modulus Ag	Y_{Ag}	83 GPa
Young modulus Au	Y_{Au}	78 GPa
shear modulus H_2O[17]	G_{H_2O}	1.3×10^{-5} N/m^2
bulk modulus H_2O	K_{H_2O}	2.15×10^{9} N/m^2
linear expansion coefficient Ag	α_{Ag}	18.9×10^{-6} 1/K
linear expansion coefficient Au	α_{Au}	14.2×10^{-6} 1/K
linear expansion coefficient H_2O	α_{H_2O}	70×10^{-6} 1/K
heat capacity Ag	c_{Ag}	230 J/kg/K
heat capacity Au	c_{Au}	129 J/kg/K
heat capacity H_2O	c_{H_2O}	4200 J/kg/K

The $\boldsymbol{s}$ and $\boldsymbol{\epsilon}$ are defined as the total stress and total strain tensors and α is the thermal expansion tensor, T and T_0 are the temperature and a reference temperature, and $\boldsymbol{C}$ is the fourth-order elasticity tensor related to shear and bulk modulus; ":" stands for the double-dot product (or double contraction). To evaluate PA pressure generation in close vicinity of the NP, water will be treated as a solid domain with bulk and shear modulus.[17] The stress tensor, $\boldsymbol{s}$, is related to the second derivative of the structural displacement, $\boldsymbol{u}$, with respect to time and defined at the domain

$$\nabla \mathbf{s} = \rho \frac{\partial^2 \mathbf{u}}{\partial t^2} \tag{6}$$

On the boundary between the water and NP and the boundary between water (thermal expansion) and water (pressure wave propagation), the normal acceleration for the acoustic pressure, p_t, equals to the acceleration, based on the second time derivative of the structural displacement

$$\mathbf{n} \cdot \left(\frac{1}{\rho} \nabla p_t \right) = -\mathbf{n} \cdot \frac{\partial^2 \boldsymbol{u}}{\partial t^2} \tag{7}$$

where $\mathbf{n}$ is the outward normal to the boundary (see Figure 1a).

Acoustic Wave Propagation. The PA wave generation by either thermal expansion of Au−Ag alloy NP or surrounding medium and propagation in an optically heterogeneous medium is described by the following acoustic wave equation

$$\frac{1}{\rho c_s^2} \frac{\partial^2 p_t}{\partial t^2} - \nabla \frac{1}{\rho} (\nabla p_t) = 0 \tag{8}$$

where c_s is the speed of sound and $p_t = p + p_b$ is the total acoustic pressure. (p is the sound pressure and p_b is the ambient pressure.)

Table 1 lists all of the parameters used in the FE model of the NP-based PA response simulation.

SIMULATION METHODOLOGY

The COMSOL Multiphysics software package is used to solve a fully coupled system of partial differential equations (PDEs) self-consistently in three dimensions using the FE method. These PDEs include the distribution of the electromagnetic field (stationary problem of radio frequency (RF) module in COMSOL), thermal response of the NP and the surrounding medium (transient problem of heat-transfer module in COMSOL), thermo-elastic response of the system (transient problem of structural mechanics module in COMSOL), and finally the acoustic pressure wave propagation (transient problem of acoustics module in COMSOL). To do this we introduce three concentric spherical domains where on the outer surface of the third domain (surrounding environment) the PA signals are calculated as a function of time due to the photothermal expansion of the first (the NP) and the second (the immediate surrounding environment) domain (see Figure 1a).

In our simulation, the following coupling variables are used: Resistive heating due to electromagnetic wave interaction with alloy NP is used in heat transfer analysis to represent heat source of the Gaussian laser pulse; temperature rise in the alloy NP and surrounding medium is used in linear elastic thermal expansion calculations of the NP and water domain in structural mechanics analysis; and pressure wave generated by thermal expansion of the NP and water is used as a boundary coupling parameter between structural mechanics and acoustics simulations.

Additional boundary and domain conditions are used to truncate size of the domain in model's geometry. Perfectly matched layer (PML) and absorbing boundary condition is used in electromagnetic wave simulation to truncate and eliminate reflections from the boundary. Spherical wave radiation boundary condition is used in the acoustics simulations to allow an outgoing spherical pressure wave to leave the modeling domain with minimal reflections (see Figure 1b).

DOI: 10.1021/acs.jpcc.5b08359
J. Phys. Chem. C XXXX, XXX, XXX−XXX

RESULTS AND DISCUSSION

RF Analysis. In Figure 2, the absorption spectrum of the Au−Ag alloy NP in an aqueous medium, with GMF = 0.55 and

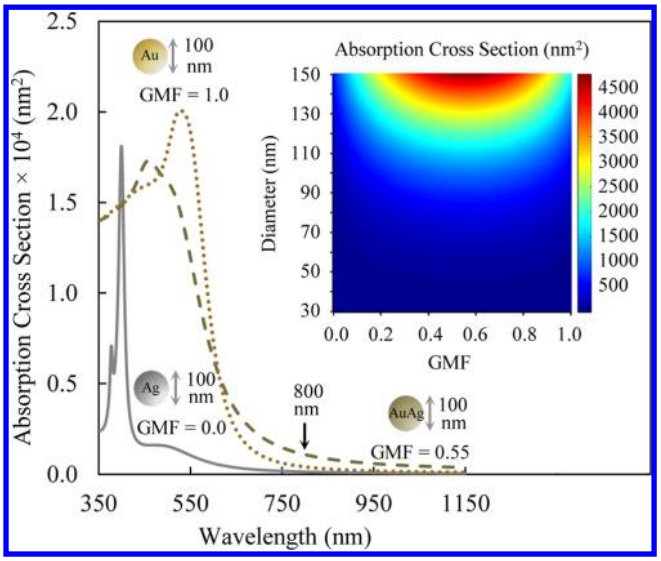

Figure 2. FE model calculation of absorption cross sections as a function of the incident laser wavelength for 100 nm AgNP (solid line), Au−Ag alloy NP (dashed line), and AuNP (dotted line) with GMF = 0, GMF = 0.55, and GMF = 1, respectively. The inset shows the absorption cross-section in color map versus the NP's GMF and diameter, in which an incident light with the wavelength of 800 nm irradiates the NP.

diameter = 100 nm, is compared with that of pure AuNP (GMF = 1, diameter = 100 nm) and pure AgNP (GMF = 0, diameter = 100 nm). The reason we chose GMF = 0.55 for the alloy is that the maximum absorption cross-section occurs at this value. (See the inset of Figure 2 in color map.) This inset shows the absorption cross-section spectrum versus different compositions and sizes of NPs irradiated by an incident light with the wavelength of 800 nm. In this inset, the size of the NP increases from 30 to 150 nm in diameter by steps of 1 nm, and the GMF of NPs increases from 0 to 1 by steps of 0.01. The maximum absorption cross-section in this inset is σ_{abs} = 4743 nm^2 corresponding to the Au−Ag alloy NP with a diameter of 150 nm and GMF = 0.55. The absorption cross-section at 800 nm is related to the imaginary part of the dielectric function of the metal at 800 nm. For Au−Ag alloys, the main contribution to the dielectric function at this wavelength comes from the free electrons. For the alloys, the effect of the disorder of the Au and Ag atoms results in a decrease in the mean free path of the electrons, which itself results in an increase in the imaginary part of the dielectric function. This means that in alloys, the free electrons transfer their energy to the lattice more efficiently compared with pure metals. Therefore, the absorption is more effective in alloys and the disordering is maximized with a GMF = 0.55.

The absorption cross-section can further increase with the increase in the size of the particle above 150 nm; however, we limited our calculations to this range of particle sizes (30−150 nm in diameter) because the experimental Au−Ag alloy NPs have been only demonstrated up to 150 nm diameters.[9] Furthermore, for considerations of mobility in the biological organism, it is preferable to limit the size of the NPs.

In Figure 2, on the AgNP absorption spectrum two absorption peaks are shown that correspond to the dipole and quadrupole plasmon resonances.[18] As the GMF of NPs increases, the position and intensity of the plasmon resonance peak of these particles change and the contribution of the quadrupole plasmon resonance decreases, while the dipole plasmon resonance peak broadens and shifts slightly toward the longer wavelength (red shift). It is important to note that for the off-resonance irradiation, in our case at λ = 800 nm, the absorption cross-section is relatively small compared with that in shorter wavelengths. As a result, by choosing an appropriate fluence for the incident pulsed laser, the thermal energy absorption by NPs at λ = 800 nm can be controlled not to cause any fragmentation, deformation, or melting of NPs, ensuring that the NPs remain intact. The experimental extinction spectra of Au−Ag alloy NPs with compositions varying from GMF = 0 to 1 in 10% GMF increments can be found in ref 9.

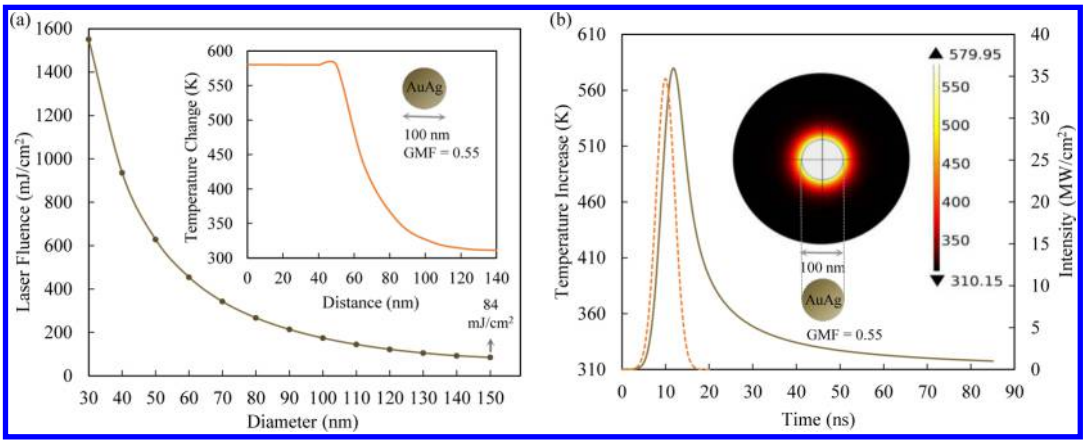

Figure 3. (a) Maximum laser fluence applicable on different sizes of spherical Au−Ag alloy NP with GMF = 0.55 in water and irradiated by a 5 ns pulsed laser at 800 nm. The inset shows the distribution of temperature around Au−Ag alloy NPs with diameter of 100 nm and GMF = 0.55 as a function of the distance from the NP center. (b) Temperature variation on the surface of a spherical Au−Ag alloy NP with diameter of 100 nm and GMF = 0.55, embedded in water, and irradiated by a 5 ns, 173.5 mJ/cm^2 pulse at 800 nm (solid line). The dotted line shows the time intensity profile of the laser as a secondary axis. The inset shows the temperature in color map for the Au−Ag alloy NP with a diameter of 100 nm and GMF = 0.55 at the maximum possible temperature of 580 K.

DOI: 10.1021/acs.jpcc.5b08359
J. Phys. Chem. C XXXX, XXX, XXX−XXX

Please note that in practice the NPs can be produced with only citrate on the surface, which should have a negligible effect on their properties. The use of larger ligands and antibodies for functionalization could affect the results; however, the main result that alloys with a GMF = 0.55 to give the best absorption should not be affected by the presence of the ligands.

Thermal Analysis. We restrict our calculations to avoid any phase change at the particle surface/water interface. By numerically solving eq 3, the temperature distribution inside the NP and the surrounding medium was calculated. The thermal analysis was performed to determine the laser fluence that increases the temperature of the NP/water interface from its initial value of 310 K to the threshold temperature of 580 K = 0.9 × $T_{critical.}$ $T_{critical}$ is the critical temperature required for evaporation and phase change at NP/water interface.[13]

In Figure 3, we show the impact of the incident laser fluence on the temperature increase in and around the NP. Figure 3a shows the maximum 5 ns pulsed laser fluence that one can safely apply on Au−Ag alloy NPs of various sizes with GMF = 0.55, without reaching the threshold temperature at the NP/water interface. We chose to calculate the maximum fluence at GMF = 0.55 because the maximum temperature at any size of NP, irradiated by a 5 ns pulsed laser at wavelength of 800 nm, occurred at this alloy composition. As seen in this Figure, the maximum fluence decreases substantially by increasing the particle's size. To get a sense of the heat penetration depth around the NP/water interface at the maximum value of the temperature (580 K), see the inset of Figure 3a, where we show the distribution of temperature for an Au−Ag alloy NP (GMF = 0.55, diameter =100 nm) as a function of distance from the particle center. As seen in this inset, the temperature has dropped drastically close to the initial value (310 K), at the distance equal to twice the radius of the Au−Ag alloy NP (50 nm in radius). Figure 3b shows the thermal evolution profile for Au−Ag alloy NPs with size of 100 nm in diameter and GMF = 0.55, irradiated by a 5 ns pulsed laser with the maximum safe fluence of 173.5 mJ/cm^2 at 800 nm. The pulse intensity profile versus time is also shown as a dotted line. As seen in this Figure, there is a time delay of ∼3 ns between the intensity peak and the temperature peak at 580 K. In addition, ∼70 ns after the intensity reaches its maximum, the temperature of surface/water interface gets back down to its initial value. The inset of Figure 3b shows the temperature in color map at the maximum possible temperature of the Au−Ag alloy NP with diameter of 100 nm and GMF = 0.55.

Photoacoustic Analysis. In Figure 4, time-domain PA signal and its corresponding Fast Fourier Transform (FFT) spectrum are shown for AgNPs (GMF = 0), Au−Ag alloy NPs (GMF = 0.55), and AuNPs (GMF = 1) with diameters equal to 100 nm. We chose to measure the PA signal with an alloy with GMF = 0.55, where the maximum thermal energy deposition in the particle occurs. To have a better comparison between the values obtained from NPs of different GMFs, we normalized both PA pressure and amplitude (FFT spectrum) to the maximum PA pressure and amplitude obtained from the NP with GMF = 0.55. As seen in this Figure, the amplitude of PA signal obtained from Au−Ag alloy NPs at GMF = 0.55 is about 10 and 2.5 times bigger than that obtained from AgNPs and AuNPs, respectively. At the FFT spectrum, the maximum amplitude for all three NPs occurs at the frequency of 65 MHz. Also, to confirm that choosing the GMF = 0.55 leads to achieving the maximum PA pressure signal, we ran our simulation for two more intermediate GMFs (0.45 and 0.65), shown in Figure 4.

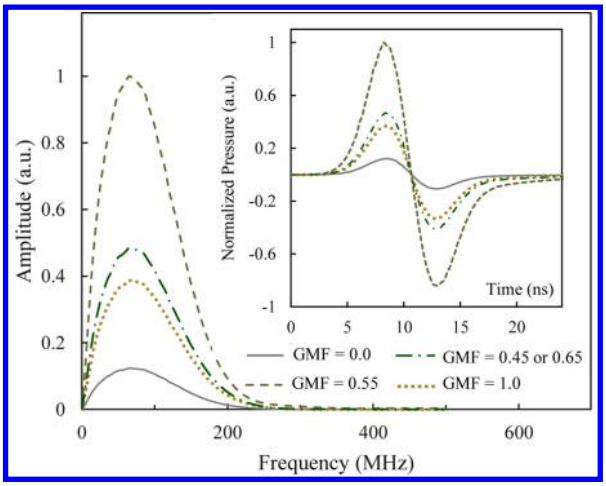

Figure 4. Normalized FFT spectrum of the acoustic pulse measured on NPs with diameter of 100 nm and GMFs of 0, 0.45, 0.55, 0.65, and 1. The inset shows the normalized time-domain acoustic pulse out of which the FFT spectrum has been measured.

Figure 5 represents the normalized acoustic pressure for AgNPs (GMF = 0), Au−Ag alloy NPs (GMF = 0.55), and AuNPs (GMF = 1) in water for NP diameters ranging from 30 to 150 nm, where the NPs are irradiated by 5 ns pulsed laser with fluence of 84 mJ/cm^2 at λ = 800 nm. Note that the fluence of 84 mJ/cm^2 is the maximum fluence that can safely be applied to all NP sizes without reaching the critical temperature at the NP/water interface (see Figure 3). Figure 5 shows that PA pressure signal for NPs of all three GMFs increases with the size of the NPs. In addition, it shows that the biggest signal corresponding to each size comes from the Au−Ag alloy NP with the GMF of 0.55 and not from the pure gold or silver.

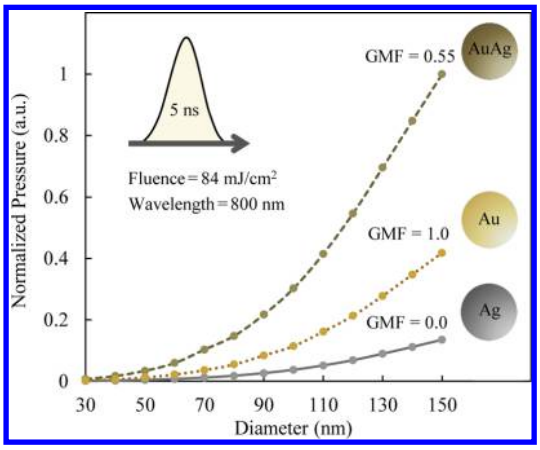

Figure 5. FE model calculation of normalized acoustic pulse versus the size of NPs with diameters ranging from 30 to 150 nm and GMFs of 0.0, 0.55 and 1.0, irradiated by 5 ns pulsed laser with wavelength of 800 nm and at the threshold fluence of 84 mJ/cm^2.

Please note that in this paper the PA response from only one NP is calculated. We expect the PA signal from aggregated NPs to be greatly enhanced in comparison with disperse NPs. This aggregation in practice is due to the cellular uptake and endocytosis of NPs.[19]

DOI: 10.1021/acs.jpcc.5b08359
J. Phys. Chem. C XXXX, XXX, XXX−XXX

CONCLUSIONS

We presented a numerical framework to study the spherical gold−silver alloy NPs (Au−Ag alloy NPs) as contrast agents for PA imaging applications. The use of these Au−Ag alloy NPs as the PA signal enhancement was compared against pure AgNPs and AuNPs with the same geometries and initial conditions. NPs of different sizes and Au−Ag compositions in this study were all in water and were irradiated by a nanosecond pulsed laser in the tissue therapeutic optical window (wavelength = 800 nm). While the NPs showed an increase in their absorption cross-section along with an increase in their sizes, they all had the maximum in absorption cross-section in the composition with GMF of 0.55. The acoustic pressure signal followed a similar trend and increased with an increase in NP's size, while it attained a highest value at the GMF = 0.55 compared with the GMFs of 1 and 0. The maximum fluence to safely use NPs with GMF = 0.55 of any size ranging from 30 to 150 nm in diameter was also calculated. Overall, the results showed that the Au−Ag alloy NPs can be used as PA imaging contrast agents with a higher PA signal generation than can be obtained from pure AuNPs and AgNPs. Therefore, these particles can be considered as a reliable contrast agent in PA imaging technique and can improve the contrast of the images much more than the commonly used pure gold and pure silver NPs of similar size and shape.

AUTHOR INFORMATION

Corresponding Author

*Phone: (705) 474-3450, ext. 4659. E-mail: alih@nipissingu.ca.

Notes

The authors declare no competing financial interest.

ACKNOWLEDGMENTS

We thank Nipissing University for the financial support through Start-Up Research Grant (SURG) and Internal Research Grant (IRG).

ABBREVIATIONS

FE, finite element; PA, photoacoustic; NP, nanoparticle; NIR, near-infrared; GMF, gold molar fraction; LSPR, localized surface-plasmon resonance; PDEs, partial differential equations; fwhm, full width at half-maximum; RF, radio frequency; PML, perfectly matched layer; FFT, fast Fourier transform

REFERENCES

(1) Wu, D.; Huang, L.; Jiang, M.; Jiang, H. Contrast Agents for Photoacoustic and Thermoacoustic Imaging: A Review. *Int. J. Mol. Sci.* **2014**, *15*, 23616−23639.

(2) Garcia, M. A. Surface Plasmons in Metallic Nanoparticles: Fundamentals and Applications. *J. Phys. D: Appl. Phys.* **2011**, *44*, 283001.

(3) Chen, Y.-S.; Frey, W.; Kim, S.; Kruizinga, P.; Homan, K.; Emelianov, S. Silica-Coated Gold Nanorods as Photoacoustic Signal Nanoamplifiers. *Nano Lett.* **2011**, *11*, 348−354.

(4) Eghtedari, M.; Oraevsky, A.; Copland, J. A.; Kotov, N. A.; Conjusteau, A.; Motamedi, M. High Sensitivity of in Vivo Detection of Gold Nanorods Using a Laser Optoacoustic Imaging System. *Nano Lett.* **2007**, *7*, 1914−1918.

(5) Skrabalak, S. E.; Chen, J.; Sun, Y.; Lu, X.; Au, L.; Cobley, C. M.; Xia, Y. Gold Nanocages: Synthesis, Properties, and Applications. *Acc. Chem. Res.* **2008**, *41*, 1587−1595.

(6) Li, M.-L.; Wang, J. C.; Schwartz, J. A.; Gill-Sharp, K. L.; Stoica, G.; Wang, L. V. In-Vivo Photoacoustic Microscopy of Nanoshell Extravasation from Solid Tumor Vasculature. *J. Biomed. Opt.* **2009**, *14*, 010507−3.

(7) Homan, K. A.; Souza, M.; Truby, R.; Luke, G. P.; Green, C.; Vreeland, E.; Emelianov, S. Silver Nanoplate Contrast Agents for in Vivo Molecular Photoacoustic Imaging. *ACS Nano* **2012**, *6*, 641−650.

(8) Weissleder, R. A Clearer Vision for in Vivo Imaging. *Nat. Biotechnol.* **2001**, *19*, 316−317.

(9) Rioux, D.; Meunier, M. Seeded Growth Synthesis of Composition and Size-Controlled Gold−Silver Alloy Nanoparticles. *J. Phys. Chem. C* **2015**, *119*, 13160−13168.

(10) Rioux, D.; Vallières, S.; Besner, S.; Muñoz, P.; Mazur, E.; Meunier, M. An Analytic Model for the Dielectric Function of Au, Ag, and Their Alloys. *Adv. Opt. Mater.* **2014**, *2*, 176−182.

(11) Patskovsky, S.; Bergeron, E.; Rioux, D.; Simard, M.; Meunier, M. Hyperspectral Reflected Light Microscopy of Plasmonic Au/Ag Alloy Nanoparticles Incubated as Multiplex Chromatic Biomarkers with Cancer Cells. *Analyst* **2014**, *139*, 5247−5253.

(12) Davletshin, Y. R.; Kumaradas, J. C. In *Finite Element Analysis of Photoacoustic Response from Gold Nanoparticle*; COMSOL: Boston, 2013.

(13) Vogel, A.; Venugopalan, V. Mechanisms of Pulsed Laser Ablation of Biological Tissues. *Chem. Rev.* **2003**, *103*, 577−644.

(14) Furlani, E. P.; Karampelas, I. H.; Xie, Q. Analysis of Pulsed Laser Plasmon-Assisted Photothermal Heating and Bubble Generation at the Nanoscale. *Lab Chip* **2012**, *12*, 3707−3719.

(15) Govorov, A. O.; Zhang, W.; Skeini, T.; Richardson, H.; Lee, J.; Kotov, N. A. Gold Nanoparticle Ensembles as Heaters and Actuators: Melting and Collective Plasmon Resonances. *Nanoscale Res. Lett.* **2006**, *1*, 84−90.

(16) Comsol Multiphysics, Acoustic Module User's Guide,Version 4.3b, 2013.

(17) Korenchenko, A. E.; Beskachko, V. P. Determining the Shear Modulus of Water in Experiments with a Floating Disk. *J. Appl. Mech. Tech. Phys.* **2008**, *49*, 80−83.

(18) Zhou, F.; Li, Z.-Y.; Liu, Y.; Xia, Y. Quantitative Analysis of Dipole and Quadrupole Excitation in the Surface Plasmon Resonance of Metal Nanoparticles. *J. Phys. Chem. C* **2008**, *112*, 20233−20240.

(19) Bayer, C. L.; Nam, S. Y.; Chen, Y.-S.; Emelianov, S. Y. Photoacoustic Signal Amplification through Plasmonic Nanoparticle Aggregation. *J. Biomed. Opt.* **2013**, *18*, 016001−016001.

DOI: 10.1021/acs.jpcc.5b08359
J. Phys. Chem. C XXXX, XXX, XXX−XXX